

Correction of misalignment errors in stereoscopic PIV systems

Rosaria Giordano^{*}, Tommaso Astarita, Giovanni Maria Carlomagno

DETEC University of Naples "Federico II"
p.le Tecchio 80, 80125 Naples, Italy

ABSTRACT

The main purpose of the present work is to correct errors occurring in a stereoscopic PIV system and caused by misalignments between the calibration plane and the measurement plane.

The experimental measurements have been conducted using an angular stereoscopic system with Scheimpflug conditions and a PIV-calibration pattern has been mounted on stages which can translate in three dimensions and rotate around the vertical axis. In order to correct the errors in perspective, a calibration of the cameras has been done by setting the PIV-calibration pattern in different z -positions and utilizing different mapping functions of the physical plane coordinates (x, y, z) ; afterwards, a cross-correlation of the images recorded by the two cameras at the same instant has been used to calculate the disparity map and to obtain the equation of the measurement plane, i.e. an estimated value of the misalignment; finally, a reconstruction of the three-dimensional displacement field has been made: in this reconstruction the image has been de-warped inside the iterative deformation PIV process, in order to reduce the loss of image quality.

A displacement field has been simulated to show the efficiency of the correction of misalignment errors. A correction of the formulae generally used in literature to estimate the viewing angles permits to obtain better results even for out of plane displacements.

1. INTRODUCTION

The Stereo-PIV technique allows to obtain three-component planar velocity measurements with Particle Image Velocimetry. Nowadays, there are different methods to implement this technique; Prasad¹ subdivided these methods into geometric and calibration-based approach. The most accurate method is the calibration-based one and it is also the most popular. It is possible to subdivide this method in further approaches: the first is based on the procedure introduced by Willert² and the second is the one proposed by Soloff et al.³. In Willert's approach, the reconstruction of three-dimensional displacement field is done by means of geometrical considerations. According to the Soloff's approach, on the other hand, 3-D vectors are obtained by means of mathematical relations.

In both methods accurate calibration, which permits to correct the error in perspective and the distortion caused by the lenses, is essential to obtain good results in measurements of the velocity components. Typically, calibration is made setting a PIV-calibration pattern, which contains a grid of marks regularly spaced along two orthogonal directions, in one or more positions along the z direction (orthogonal to the plane); ideally, the position $z = 0$ is the position of the light sheet, i.e. the measurement plane. In calibration procedure, a mapping function is obtained which allows to transform the object coordinates (x, y, z) into the image coordinates (X_1, Y_1) of camera 1 and (X_2, Y_2) of camera 2; coefficients of the mapping function are calculated with the least squares method.

At the moment, different models of calibration are used. One of these is the calibration with *camera pinhole model*, originally proposed by Tsai⁴. Another kind of calibration is the one which uses an interpolating function, e.g. a polynomial function of second order in z and of third order in x and y (Soloff³). In order to evaluate the best method to make the calibration, in the present work different calibration models have been used and compared.

The main drawback of Stereo-PIV technique is the impossibility to set the laser sheet exactly in the $z = 0$ position. A correcting procedure based on a cross-correlation between the images of cameras 1 and 2, relative to the same instant, has been proposed by many authors (Willert², Coudert and Schon⁵, Wieneke⁶). The present study compares the results obtained with and without this correction, using the reconstruction of the three-dimensional displacement field proposed by Willert.

* E-mail: r.giordano@unina.it

Web site: www.detec.unina.it

For this kind of reconstruction, as mentioned above, geometrical considerations are required, i.e. local viewing angles of each camera in every point of the measurement plane. Also in this case, different formulae have been proposed in the past. This study proposes new formulae to obtain a better reconstruction of 3-D vectors.

2. EXPERIMENTAL APPARATUS

Experiments are carried out in an angular stereoscopic PIV system, consisting of: two CCD cameras (PCO Sensicam) with a resolution of 1280x1024 pixels and 12 bits are used to record the images; PIV-calibration pattern containing both the equi-spaced dots to make the calibration and the synthetic particles to simulate the displacement field (see Fig. 1); three translational stages, which allow to shift the PIV-calibration pattern in the three directions (x , y , z), with precision of $10\mu\text{m}$; one rotational stage, which permits to rotate the PIV-calibration pattern along the y (vertical) direction with precision of $1/60^\circ$.

The viewing angles of the two cameras are -45° and 45° and, in order to obtain uniform focusing, the Scheimpflug condition is satisfied. The FOV is $125 \times 100\text{mm}$, consequently the mean spatial resolution is about $10\text{px}/\text{mm}$.

The PIV-calibration pattern is generated by a synthetic PIV pattern generator and contains dots for calibration spaced of 5mm along both the x and y directions.

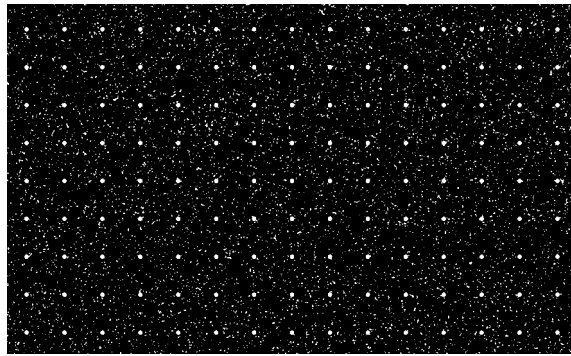


Fig. 1 – PIV-calibration pattern.

3. PROCEDURE

In this study the reconstruction of the three-dimensional displacement field based on the method proposed by Willert² has been carried out. This method can be applied in following two approaches (Coudert and Schon⁵): *mapping* and *warping*. In the former approach the images are first de-warped, by using the mapping function obtained in the calibration step, then a standard PIV algorithm is applied to both images on a common grid to compute the two-component displacement field for each camera. In the warping approach, the 2-D displacement fields are evaluated on different irregular grids for the two cameras and, then, projection by means of mapping functions and interpolation of vectors on the object plane are made. For both approaches, the 3-D displacement field is determined afterwards by means of a stereoscopic reconstruction. The advantage of the warping method is the smaller computational time with respect to the mapping one. However, with the warping approach, the field of 2D vectors is smoothed, as it is obtained interpolating the vector maps on a common regular grid, and the spatial resolution is non-uniform and non-isotropic, as the cross-correlation is done on warped images. The disadvantage of the mapping method, instead, is the need of image re-sampling, and consequently the loss of images quality.

In this study the mapping approach is adopted, with a further precaution, in order to reduce the loss of image quality and, then, of the 3D displacement field: de-warping of the images is achieved inside the iterative deformation PIV process, according to Scarano et al.⁷ and Wieneke⁸.

The scheme of the whole procedure adopted is shown in Fig. 2 and consists of the following steps:

1. An achievement of Scheimpflug condition is done in order to ensure an uniform focalization of images.
2. Calibration is achieved to correct errors in perspective and distortions caused by lenses: a mapping function which transforms the object coordinates (x , y , z) into the image coordinates (X_1, Y_1) of camera 1 and (X_2, Y_2) of camera 2 is computed (see Sec. 3.1).
3. The disparity map is evaluated by de-warping and then cross-correlating the images recorded by the two cameras in the same instant (see Sec. 3.2), and the measurement plane equation is computed by means of a regression method.
4. Iterative Deformation PIV Process is done on each couple of de-warped images: de-warping of images is done inside the process, by taking into account the real position of the measurement plane.

5. Geometric reconstruction of the three-dimensional displacement field is obtained by means of the two 2-D vectors field (related to the two cameras) and of the local viewing angles (see Sec. 3.3).

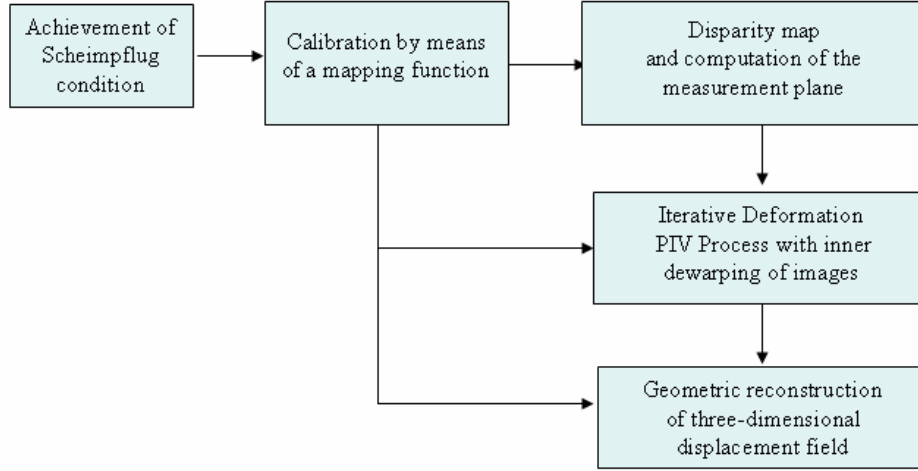


Fig. 2 – Procedure of Stereo-PIV adopted.

3.1 Calibration

As mentioned before, nowadays different models of calibration are used: camera pinhole model and calibration based on interpolating function. The camera pinhole model is made up of 6 extrinsic and 6 intrinsic parameters. The first ones describe the position of camera pinhole in object space by means of a translation vector and a rotation matrix. Intrinsic parameters are specific to the camera: pixel aspect ratio; radial distortion factors (first and second order) which describe the distortion caused by the lenses; focal length; intersection of the optical axis with the image plane. In order to apply the second type of calibration, it is possible to choose a generic interpolating function. In the literature there are a lot of examples: polynomial functions of second order in z and third order in x and y (Soloff³); polynomial function of second order in x and y (van Oord⁹), rational function of first order in x and y and rational function of second order in x and y (Willert²). In this work the following interpolating functions have been used:

- ❖ polynomial function of third order in x and y and second order in z (in the following indicated as P332):

$$\hat{F}(\underline{x}) = a_0 + a_1x + a_2y + a_3z + a_4x^2 + a_5xy + a_6y^2 + a_7xz + a_8yz + a_9z^2 + a_{10}x^3 + a_{11}x^2y + a_{12}xy^2 + a_{13}y^3 + a_{14}x^2z + a_{15}xyz + a_{16}y^2z + a_{17}xz^2 + a_{18}yz^2 \quad (1)$$

- ❖ polynomial function of third order in x , y and z (P333):

$$\hat{F}(\underline{x}) = a_0 + a_1x + a_2y + a_3z + a_4x^2 + a_5xy + a_6y^2 + a_7xz + a_8yz + a_9z^2 + a_{10}x^3 + a_{11}x^2y + a_{12}xy^2 + a_{13}y^3 + a_{14}x^2z + a_{15}xyz + a_{16}y^2z + a_{17}xz^2 + a_{18}yz^2 + a_{19}z^3 \quad (2)$$

- ❖ rational function of second order in x , y and z (R222):

$$\hat{F}(\underline{x}) = \frac{a_0 + a_1x + a_2y + a_3z + a_4x^2 + a_5xy + a_6y^2 + a_7xz + a_8yz + a_9z^2}{1 + a_{10}x + a_{11}y + a_{12}z + a_{13}x^2 + a_{14}xy + a_{15}y^2 + a_{16}xz + a_{17}yz + a_{18}z^2} \quad (3)$$

- ❖ rational function of first order in x , y and z (R111):

$$\hat{F}(\underline{x}) = \frac{a_0 + a_1x + a_2y + a_3z}{1 + a_4x + a_5y + a_6z} \quad (4)$$

and they have been compared with the camera pinhole model (CPM). It is interesting to note that the R111 model is a simplified CPM model.

For each model three and five different positions of the PIV-calibration pattern along the z direction have been used, apart for the P333 model, for which only 5 different positions have been used.

The PIV-calibration pattern used (Fig. 1) has both dots for implementing calibration and synthetic particles for simulating a displacement. The advantage of this choice is the possibility to use a single target for the whole simulation

process and, thus, to avoid possible position errors associated with the change of the pattern. However, this kind of target requested a robust procedure to find the dots in the calibration algorithm (see Fig. 3).

The calibration grid dots localisation procedure is made up of the following steps:

- ❖ Dots localisation is made by means of a threshold parameter: if the pixel grey value is greater than the mean grey value multiplied by a threshold parameter, the pixel belongs to a calibration dots.
- ❖ Elimination of wrong dots by means of geometrical considerations, e.g., the calibration dots are aligned on a line.
- ❖ Centre of dots has been localised by finding the local sub-pixel maximum.

In this way, all the calibration points in the PIV-calibration pattern have been found. Afterwards it is possible to optimise the mapping function by means of the least squares method. After that, this whole procedure is iterated in order to correct the wrong points and to find new points not found before.

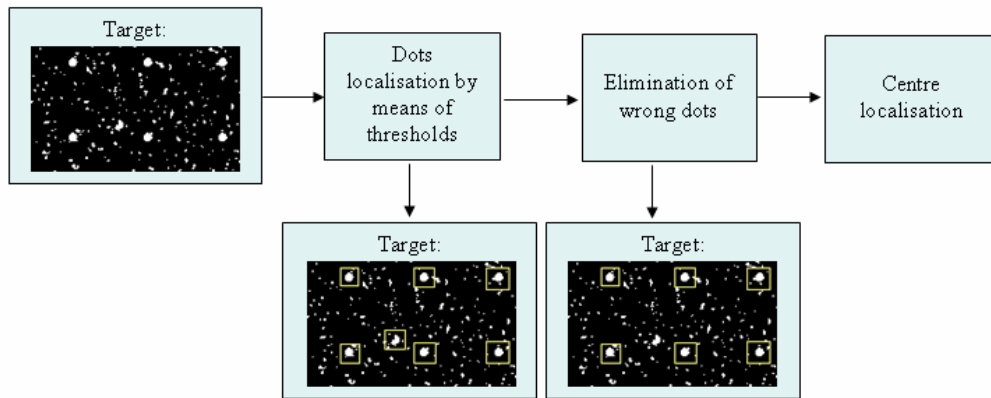


Fig. 3 – Calibration grid dots localisation procedure.

3.2 Evaluation of misalignment

One of the major drawbacks of the Stereo-PIV technique is the unavoidable misalignment error which occurs between the calibration plane and the laser sheet, i.e. the measurement plane. Generally, an offset along z direction and a rotation around x and y axis form this misalignment. If it isn't corrected, one commits the following errors:

- ❖ The two de-warped images, recorded by the two cameras in the same instant, aren't coincident, since they have been back-projected in an erroneous position. This mistake causes a fictitious additional displacement field.
- ❖ The local viewing angles have been calculated in an erroneous position, so they are wrong and cause a mistake in the evaluation of three-dimensional displacement vectors.
- ❖ The three-dimensional displacement reconstruction is made using 2D-vectors relative to two different positions.

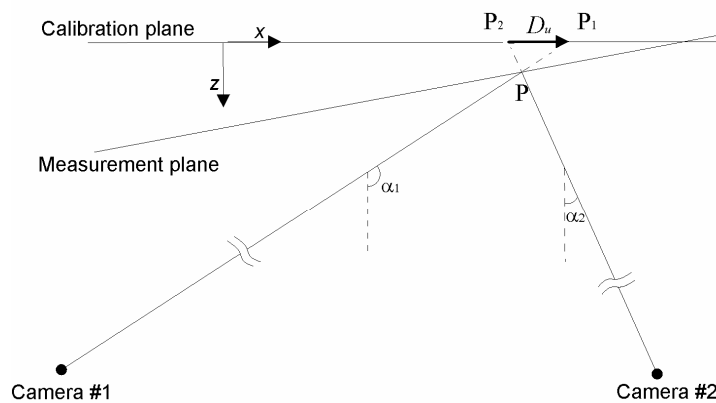


Fig. 4 – Misalignment between the calibration plane and the measurement plane.

As shown in Fig. 4, when a misalignment occurs, a generic point P of the measurement plane is viewed in two different position P₁ and P₂ by the two cameras.

Using the disparity vector and the local viewing angles, it is possible to compute the local misalignment, by means of a triangulation method:

$$z_{meas} = z_{calib} + \frac{D_u}{\tan \alpha_1 + \tan \alpha_2} \quad (5)$$

By cross-correlating the two de-warped images of the cameras, recorded in the same instant, it is possible to compute a disparity map and the equation of the measurement plane in the object space can be computed by means of a regression method.

3.3 Geometric reconstruction of three-dimensional displacement field

The reconstruction of the three-dimensional displacement field is achieved using the two 2D displacement fields calculated by means of a PIV process made on the two couples of images recorded by the two cameras. As mentioned before, in the present study the reconstruction proposed by Willert² has been adopted. This procedure permits to calculate the three components of the particles' displacement, dx , dy , dz , from the two-dimensional displacements dx_1 , dy_1 , dx_2 , dy_2 (the indices 1 and 2 refer to camera 1 and 2 respectively), by means of geometrical considerations, as shown in Fig. 5. The same figure also shows the local viewing angles α_1 , α_2 , β_1 and β_2 , useful for the 3-D reconstruction.

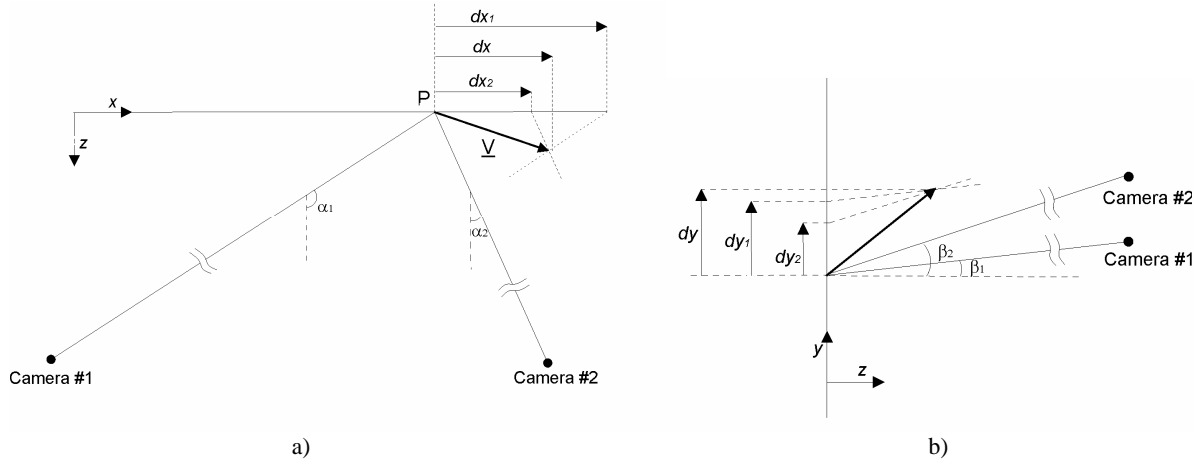


Fig. 5 – Geometric description used for reconstruction of 3D-displacement field: a) x-z plane; b) y-z plane.

The formulae used herein are the ones proposed by Willert:

$$dx = \frac{dx_1 \operatorname{tg} \alpha_2 - dx_2 \operatorname{tg} \alpha_1}{\operatorname{tg} \alpha_2 - \operatorname{tg} \alpha_1} \quad (6)$$

$$dz = \frac{dx_1 - dx_2}{\operatorname{tg} \alpha_2 - \operatorname{tg} \alpha_1} = \frac{dy_1 - dy_2}{\operatorname{tg} \beta_2 - \operatorname{tg} \beta_1} \quad (7)$$

$$dy = \frac{dy_1 \operatorname{tg} \beta_2 - dy_2 \operatorname{tg} \beta_1}{\operatorname{tg} \beta_2 - \operatorname{tg} \beta_1} = \frac{dy_1 + dy_2}{2} + \frac{dz}{2} (\operatorname{tg} \beta_1 + \operatorname{tg} \beta_2) \quad (8)$$

Willert in 1997 evaluated the viewing angles by measuring the relative distances:

$$\tan(\alpha_1) = \frac{x_P - x_1}{z_P - z_1} \quad \tan(\alpha_2) = \frac{x_P - x_2}{z_P - z_2} \quad (9)$$

$$\tan(\beta_1) = \frac{y_P - y_1}{z_P - z_1} \quad \tan(\beta_2) = \frac{y_P - y_2}{z_P - z_2} \quad (10)$$

where (x_P, y_P, z_P) , (x_1, y_1, z_1) and (x_2, y_2, z_2) are the coordinates in the object space of the measurement point and of the pinhole of camera 1 and camera 2, respectively (see Fig. 5).

More recently (2004), Fei and Merzkirch¹⁰ suggested formulae of the first order which make use of the mapping function:

$$\tan(\alpha_1) = \frac{dx}{dz} = \frac{X_z^{(1)}}{X_x^{(1)}} \quad \tan(\alpha_2) = \frac{dx}{dz} = \frac{X_z^{(2)}}{X_x^{(2)}} \quad (11)$$

$$\tan(\beta_1) = \frac{dy}{dz} = \frac{Y_z^{(1)}}{Y_y^{(1)}} \quad \tan(\beta_2) = \frac{dy}{dz} = \frac{Y_z^{(2)}}{Y_y^{(2)}} \quad (12)$$

where $X^{(1)}$ is the X component of vectorial mapping function related of camera 1, $Y^{(1)}$ is the Y component, and so forth; the subscript indicates derivation. In this work, second order formulae which also use the mapping function are used.

4. EXPERIMENTAL RESULTS

In this section, experimental results will be shown for each step of the Stereo-PIV procedure: for the calibration step the different models described in Sec. 3.1 will be compared; for the correction of misalignment errors, it will be proved the utility of the correction by means of a comparison between results obtained with and without correction; finally, it will be shown that the second order formulae used to estimate the viewing angles allow to obtain better results even for out of plane displacements.

4.1 Calibration

In Table 1 and Table 2 the results of different calibration models are reported for three and five different position of PIV-calibration pattern respectively.

Calibration method	RMS		MAX ERROR		R-SQUARE	
	Cam 0 - Cam 1		Cam 0 - Cam 1		Cam 0 - Cam 1	
CPM	0.3992	0.4044	1.3740	1.3030	0.9980	0.9953
P332	0.2924	0.2705	1.0380	0.9807	0.9992	0.9981
R222	0.2942	0.2712	1.0140	0.9860	0.9993	0.9982
R111	0.3865	0.3914	1.4300	1.1920	0.9952	0.9998

Table 1 - Results of calibration with 3 planes using CPM, P332, R222, R111

Calibration method	RMS		MAX ERROR		R-SQUARE	
	Cam 0 - Cam 1		Cam 0 - Cam 1		Cam 0 - Cam 1	
CPM	0.3954	0.4023	1.3770	1.3050	0.9965	0.9969
P332	0.2929	0.2736	1.0477	0.9695	0.9982	0.9980
P333	0.2923	0.2721	1.0453	0.9681	0.9983	0.9982
R222	0.2946	0.2743	1.0866	0.9751	0.9979	0.9982
R111	0.3858	0.3935	1.4197	1.1969	0.9970	0.9997

Table 2 - Results of calibration with 5 planes using CPM, P332, P333, R222, R111

For each model, it is shown the RMS and the maximum error between the real physical position and the position predicted by the mapping function. The tables also show the R-Square value, which indicates how well the residual values are approximated by a Gaussian curve. Analysing the tables it appears that the best interpolating method is the P332 applied to three planes. Unfortunately this is a high order method – it requires, in fact, the estimation of 38 parameters - and it is therefore very sensible to noise. Lower order methods, as CPM for example, are therefore more efficient, resulting in smoother functions which are less influenced by noise. The results also show that the R111 model is very close to the CPM one, as already mentioned.

It is interesting to note that the use of five planes doesn't allow to obtain better results than the use of just three planes, in spite of the major number of dots used to evaluate the interpolating function.

If the mapping function is known, it is possible to compute the local viewing angle on each object plane point. This angle is essential to obtain the three-component reconstruction, as it will be shown below.

4.2 Correction of misalignment errors

In order to show the improvements obtained with the corrections of misalignment errors, an uniform displacement field along x equal to $1mm$ with an imposed angular misalignment of the measurement plane equal to -1° is simulated. Using the procedure described in Sec. 3.2, the equation of the measurement plane has been evaluated:

$$z = 9.20e - 002 - 1.69e - 002 \cdot x + 9.51e - 006 \cdot y \quad (13)$$

Eq. 13 indicates a coefficient of x equal to -0.0169 that is equivalent to an angle of -0.969° , whereas, the coefficient of y shows a very small rotation around x -axis. Since the rotation axis doesn't coincide with y -axis of the reference frame (x, y, z), the equation shows that there is also a displacement of the measurement plane.

As shown in Table 3, since the uniform displacement along x has been done after the angular misalignment, the prediction of the displacement field component has also a w component, in addition to the u component. Means of the displacement field components indicate a remarkable error for the w component obtained without correction.

		u	v	w
Imposed		0.986	0	-0.0169
With disparity map	Mean	0.9984	-0.0005	-0.0162
	Standard deviation	0.0013	0.0009	0.0015
Without disparity map	Mean	0.9988	-0.0005	-0.0330
	Standard deviation	0.0019	0.0010	0.0015

Table 3 – 3-D displacement field components (mm) obtained with and without correction of misalignment errors.

Figs. 6, 7 and 8 show a comparison between the results obtained with and without correction of the misalignment errors for the u, v and w component of the displacement field respectively.

The map of the u component computed without correction (Fig. 7b) shows a trend along x direction with a mean value of $0.9988mm$. This trend isn't visible in the results obtained with correction (Fig. 7a), and in this case, the mean value of the component ($0.9984mm$) is smaller than the first case and also closer to the predicted value ($0.986mm$).

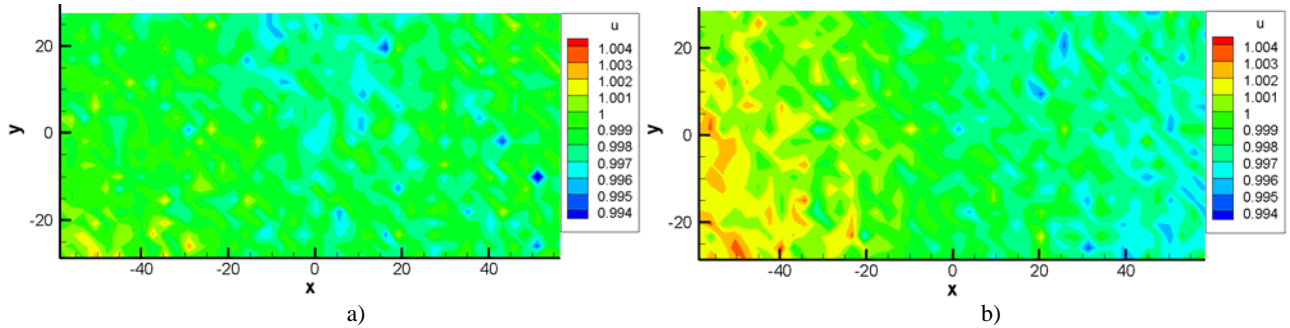


Fig. 6 – u component (mm) of 3-D displacement field obtained: a) with correction; b) without correction.

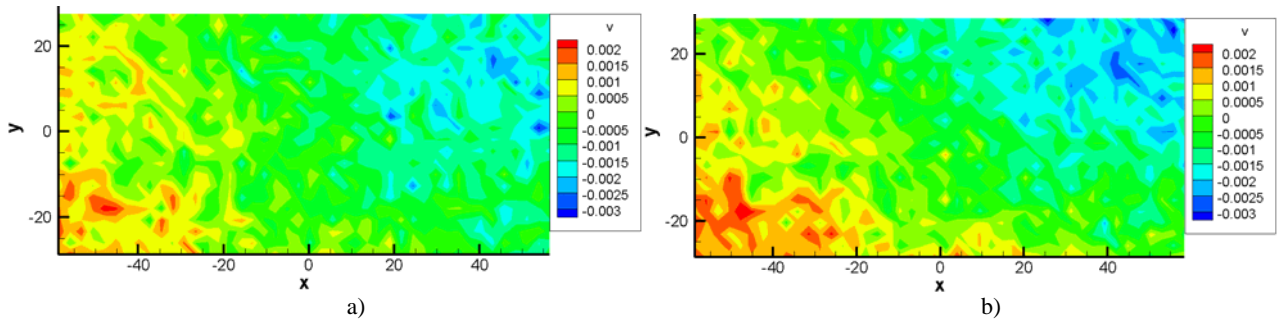


Fig. 7 – v component (mm) of 3-D displacement field obtained: a) with correction; b) without correction.

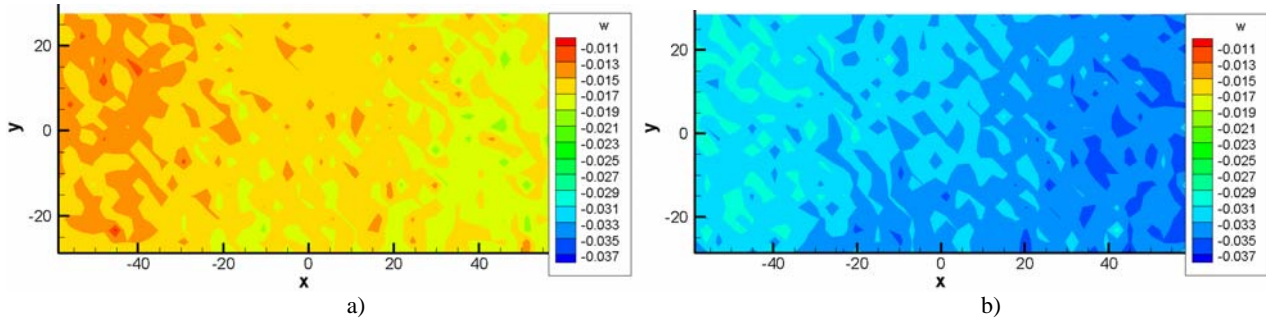


Fig. 8 – w component (mm) of 3-D displacement field obtained: a) with correction; b) without correction.

The maps of the v component (Fig. 7) show for both results a very small mean value (the imposed value is $0mm$). For the w component (Fig. 8), a significant difference is evident for the two maps, as also shown for the mean values.

4.3 Reconstruction of 3-D displacement field with second order formulae to compute viewing angles

In this section, the results relative to an uniform displacement field along z , without misalignment will be shown. This kind of displacement field has been chosen in order to confirm the improvements obtained using second order formulae to compute the local viewing angles.

For the u and w component, no remarkable differences are evident between results obtained with formulae of first and second order (see Figs. 9 and 11).

The improvements are obtained in the evaluation of the v component: the results calculated with first order formulae (Fig. 10a) show a trend along the y direction that is corrected by using the second order formulae (Fig. 10b). The trend is very significant, in fact, the value of v component belong to the interval $[-0.025, 0.025]mm$, in spite of the predictor value equal to $0mm$.

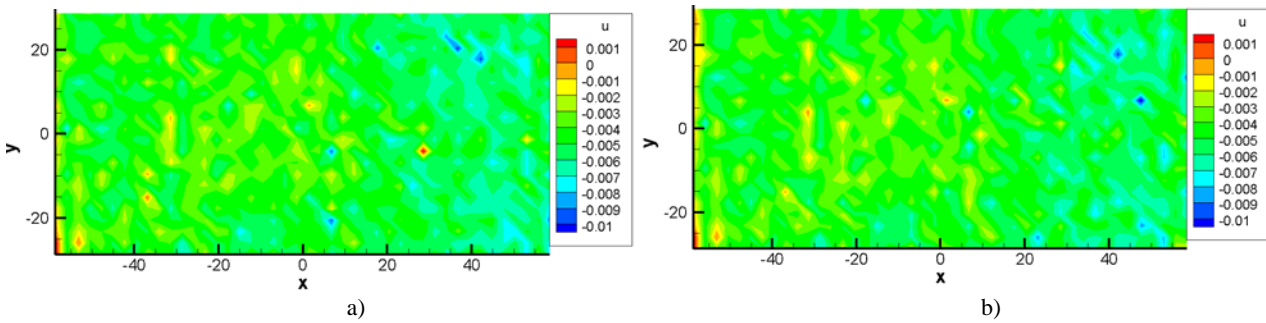


Fig. 9 – u component (mm) of 3-D displacement field obtained with formulae to compute viewing angles of: a) second order; b) first order.

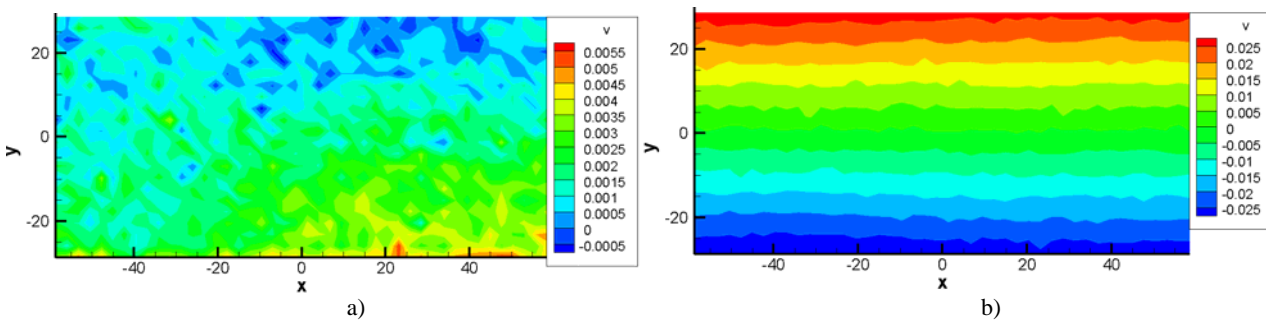


Fig. 10 – v component (mm) of 3-D displacement field obtained with formulae to compute viewing angles of: a) second order; b) first order.

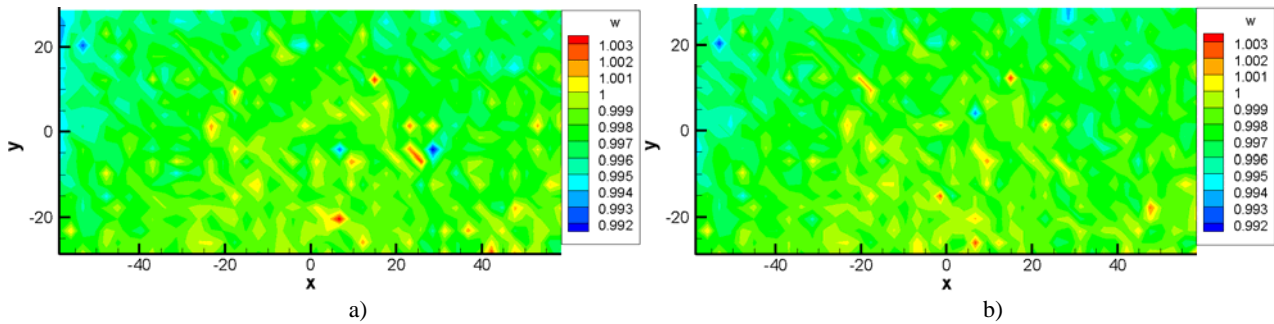


Fig. 11 – w component (mm) of 3-D displacement field obtained with formulae to compute viewing angles of:
a) second order; b) first order.

CONCLUSIONS

A stereoscopic PIV system has been applied to simulated displacement fields. The experimental measurements have been conducted using a PIV-calibration pattern mounted on stages which can translate in three dimensions and rotate around the vertical axis. A comparison between different calibration models has been conducted on three and five different positions of the PIV-calibration pattern along the z -direction and the results showed that an interpolating polynomial function of third order in x and y and second order in z is the best mapping function. In spite of the major number of dots used by the interpolating function, the use of five planes didn't produce better results.

In order to correct errors in misalignment between calibration and measurement planes, cross-correlation of images recorded by the two cameras in the same instant has been done and a disparity map has been evaluated. With a regression method, the equation of the measurement plane has been calculated. The results obtained with and without correction of misalignment errors showed the usefulness of the correction.

For the 3-D reconstruction, the method proposed by Willert has been used with an alteration: second order formulae to calculate the local viewing angle have been used. The experiments showed that these formulae permit to obtain better results, especially for out of plane displacements.

REFERENCES

1. Prasad A., "Stereoscopic particle image velocimetry", *Exp Fluids*, **29**, 103-116, 2000.
2. Willert C., "Stereoscopic digital particle image velocimetry for application in wind tunnel flows", *Meas Sci Technol*, **8**, 1465-1479, 1997.
3. Soloff S., Adrian R., Liu Z., "Distortion compensation for generalized stereoscopic particle image velocimetry", *Meas Sci Technol*, **8**, 1441-1454, 1997.
4. Tsai R.Y., "An efficient and accurate camera calibration technique for 3D machine vision", *Proceedings of the IEEE conference on computer vision and pattern recognition (CVPR '86)*, 364-374, Miami, 1986.
5. Coudert S., Schon J.P., "Back-projection algorithm with misalignment corrections for 2D3C stereoscopic PIV", *Meas Sci Technol*, **12**, 1371-1381, 2001.
6. Wieneke B., "Stereo-PIV using self-calibration on particle images", *Exp Fluids*, **39**, 267-280, 2005.
7. Scarano F., David L., Bsibsi M., Callaud D., "S-PIV comparative assessment: image dewarping+misalignment correction and pinhole+geometric projection", *Exp Fluids*, **39**, 257-266, 2005.
8. Wieneke B., "Stereo-PIV using self-calibration on particle images", *Exp Fluids*, **39**, 267-280, 2005.
9. van Oord J., "The design of a stereoscopic DPIV-system", *Delft University of thecnology report MEAH-161*, 17-18, Delft, 1997.
10. Fei R., Merzkirch W., "Investigation of the measurement accuracy of stereo particle image velocimetry", *Exp Fluids*, **37**, 559-565, 2004.